An Innovative EFD for Studying Ship Seakeeping

Hidetsugu Iwashita* **and Masashi Kashiwagi****

* Dept of Transportation & Environmental Systems, Hiroshima University, Japan
** Dept of Naval Architecture & Ocean Engineering, Osaka University, Japan

E-mail: iwashita@naoe.hiroshima-u.ac.jp, kashi@naoe.eng.osaka-u.ac.jp

1 INTRODUCTION

Recently CFD begins to be applied to seakeeping problems. However, most of the validation of computed results is based on a comparison of integrated values, i.e. wave-induced ship motions and/or hydrodynamic forces. More detailed and convincing validation is desired using local physical quantities such as ship-generated unsteady-wave pattern and spatial distribution of wave-induced unsteady pressure on the ship hull. This paper introduces an innovative measurement for the spatial distribution of unsteady pressure on a ship in waves, and obtained results are compared with corresponding results computed by Rankine Panel Method (RPM) and Enhanced Unified Theory (EUT) under the potential-flow assumption.

Employed in the present study as the sensor for measuring the pressure is the so-called FBG (Fiber Bragg Gratings) sensor, which is based on the optical-fiber sensing technology. In the experiment, more than 230 FBG pressure sensors are affixed on the starboard side of the ship-hull surface and the unsteady pressure is measured together with ship motions and added resistance, and all of measured data are Fourier analyzed at the same time. In order to validate the accuracy of the measured pressure by the FBG pressure sensors, ordinary strain-type pressure sensors are also embedded in the port side of the ship hull, and the measurement in a towing tank is carried out in both head and following wave conditions. For some test cases, the measurement is repeated at least five times, and the mean value and standard deviation of measured pressures are calculated. In connection with the added resistance in waves, the added pressure (difference of the time-averaged second-order pressure from the steady pressure in calm water) is also extracted from measured results and its contour is illustrated to show visually which region of the added pressure contributes to the added resistance.

2 FBG PRESSURE SENSOR

The FBG is a type of distributed diffraction grating etched into the fiber core that reflects particular wavelength of light, called Bragg wavelength, and transmits all others. If the spacing between reflectors changes due to variation of load, temperature and acceleration, the Bragg wavelength also changes. Therefore, the load (pressure) etc. can be measured by identifying a change in the Bragg wavelength. It is also possible to arrange many FBGs (in the order of 10~20) with different spacing of Bragg grating along one optical fiber so that the simultaneous multipoint measurement can be made.

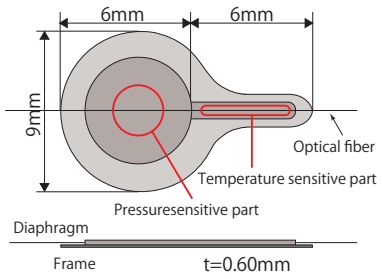

Fig. 1 FBG sensor.

Figure 1 shows a schematic diagram of the FBG pressure sensor. The size of the sensor is sufficiently small with 9 mm in diameter, 12 mm in length, and 0.6 mm in thickness. Two FBGs with different spacing of Bragg grating are contained in one sensor and they are fixed to a diaphragm so that they do not interfere with each other. One FBG measures the pressure, and the other measuring the temperature is used to compensate for temperature variation at the pressure sensitive part. The FBG sensor can be easily affixed to the hull surface by a double-sided tape.

3 TOWING TANK EXPERIMENT

The experiment was carried out using the towing tank at RIAM, Kyushu University. The ship model used in the experiment is the RIOS bulk carrier[1)], with 2.4 m in length and $C_b = 0.8$. Fig. 2 illustrates the position of the pressure sensors. Totally 234 FBG pressure sensors including 12 sensors above the still water line are affixed on the starboard side, and 19 strain-type pressure sensors are embedded in the port side to check the measurement accuracy of the FBG pressure sensors. In addition to the pressure measurement, we measured the wave-induced ship motions and added resistance in both head and following regular waves at $F_n = 0.18$ and 0.0 by using the

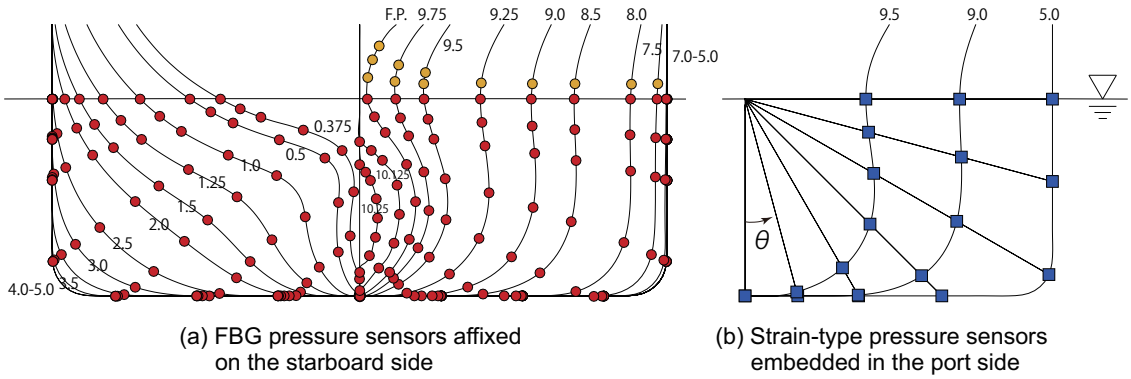

(a) FBG pressure sensors affixed on the starboard side

(b) Strain-type pressure sensors embedded in the port side

Fig. 2 Position of pressure sensors attached on RIOS bulk carrier.

motion measurement device and also hydrodynamic forces at $F_n = 0.18$ by using the forced-oscillation device; which made it possible to retrieve the pressure in the motion-free condition by a linear superposition using the results in each of the measurements.

4 NUMERICAL CALCULATIONS

To demonstrate usefulness of the measured pressure distributions, some typical numerical calculations based on the potential-flow theory are performed. The first method is the strip-theory method, and the second one is EUT developed by Kashiwagi[2]. The third one is a new RPM in the frequency domain that has been recently presented by Iwashita et al.[3]; which is based on a simplified hybrid method combining the Rankine panel method and the forward-speed Green function method, and enables calculations in the low-speed/low-frequency range where the Hanaoka's parameter $\tau = U\omega_e/g$ is smaller than 0.25, including $\tau = 0.0$. For the zero-forward speed case, the Green Function Method (GFM) is also applied as the most reliable computation method.

5 RESULTS AND DISCUSSION

5.1 Measurement Accuracy of Unsteady Pressure

Figure 3 shows the mean value and standard deviation of the unsteady pressure measured with the FBG sensors at $F_n = 0.18$, $\beta = 180$ deg and $\lambda/L = 1.25$. They are obtained by repeating the measurement for the same condition more than five times. The standard deviation illustrated by the error bar is sufficiently small and high repeatability of the measurement can be confirmed. In the amplitude, the 2nd harmonic term in the Fourier-series expansion of the pressure is illustrated together with the 1st-order term. The amplitude of 2nd harmonic term near the bow part drastically increases as the pressure sensor becomes closer to the free surface, implying significant nonlinearity near the free surface.

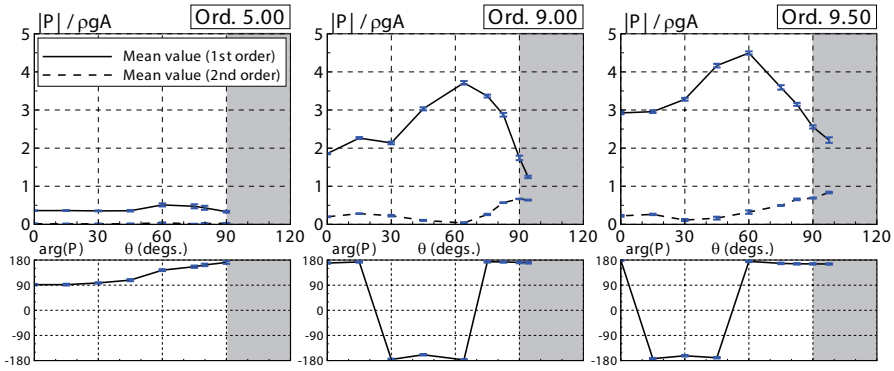

Fig. 3 Mean value and standard deviation of measured unsteady pressures at $F_n = 0.18$, $\beta = 180$ deg and $\lambda/L = 1.25$.

5.2 Zero-Forward Speed Case

Figure 4 shows the measured and computed unsteady pressure distribution at $F_n = 0.0$ and $\beta = 180$ deg, but only for $\lambda/L = 1.0$ as an example. Through comparison between measured and computed results, we can see that both GFM and RPM[3] can estimate the unsteady pressure distribution on the whole ship hull with good accuracy and hence the hydrodynamic forces and ship motions as well (although those are not shown here

due to shortage of space). It should be mentioned that Fig. 5 is an unprecedented experimental result showing clearly the spatial unsteady pressure distribution over the ship-hull surface.

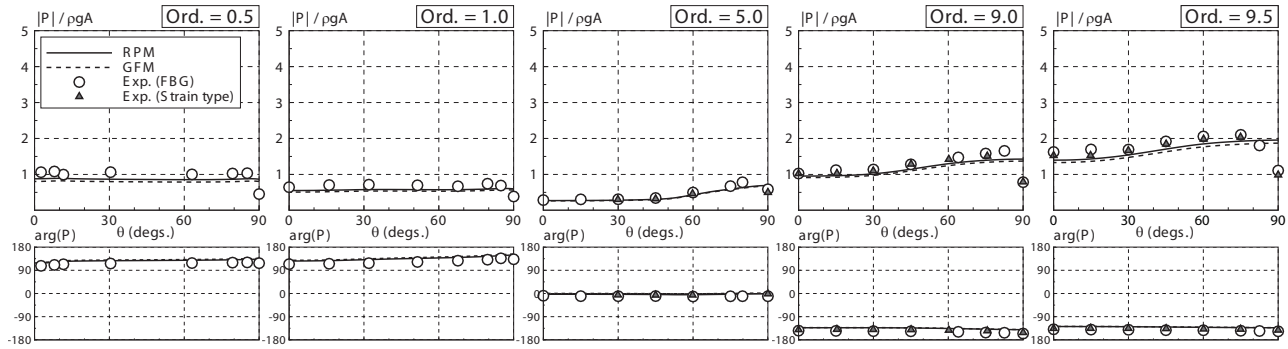

Fig. 4 Sectional unsteady pressure distribution at $F_n = 0.0$, $\beta = 180$ deg and $\lambda/L = 1.0$.

5.3 Forward Speed Case

Similar to the zero-forward speed case, Fig. 6 shows the measured and computed unsteady pressure distribution at $F_n = 0.18$, $\beta = 180$ deg. Only the case of $\lambda/L = 1.25$, which is close to the resonant frequency in ship motions, is highlighted for the unsteady pressure distribution.

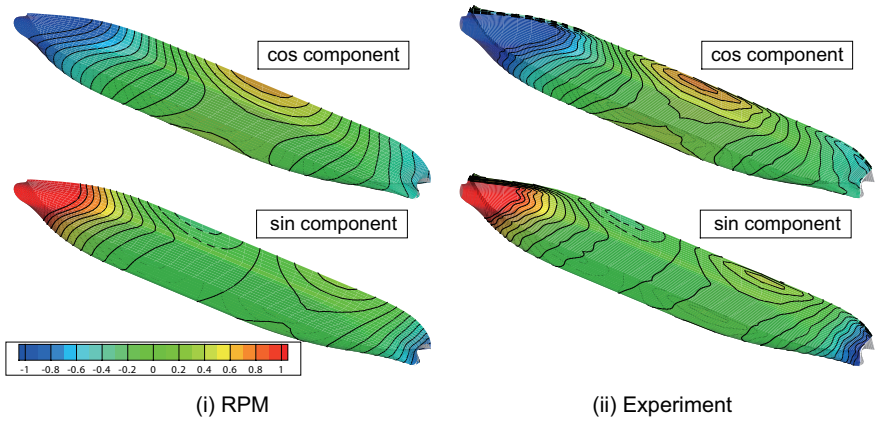

Fig. 5 Unsteady pressure distribution on the ship hull at $F_n = 0.0$, $\beta = 180$ deg and $\lambda/L = 1.0$.

Although the results of ship motions are not shown here due to shortage of space, we found that both RPM and EUT tend to overestimate the heave motion near the resonant frequency. Difference in the coupled added-mass and damping coefficients between computed and measured results may be one of the possible causes. The strip method predicts the heave and pitch motions better than the others, although 3D and forward-speed effects are not properly accounted for in the local quantities like unsteady pressure and thus hydrodynamic forces as well.

Regarding the unsteady pressure shown in Fig. 6, RPM taking account of local 3D effects is superior to the others. The color contour of the unsteady pressure in Fig. 7 is illustrated after eliminating the hydrostatic term of $p_s = -\rho g(X_3 - xX_5)$ which is directly related to heave (X_3) and pitch (X_5) motions and the discrepancy in those quantities deteriorates notably the accuracy in the pressure prediction. A comparison in Fig. 7 suggests that the hydrodynamic pressure field computed only from the velocity potential determined by RPM shows favorable agreement with measured results.

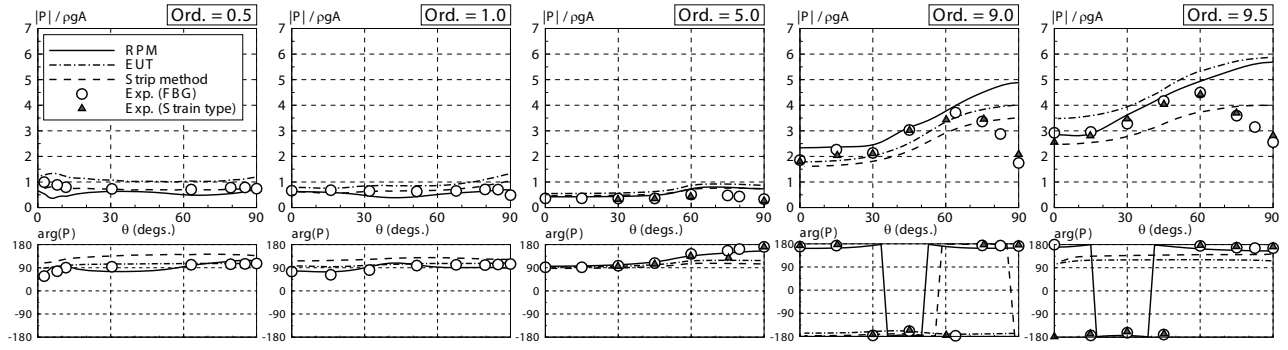

Fig. 6 Sectional unsteady pressure distribution at $F_n = 0.18$, $\beta = 180$ deg and $\lambda/L = 1.25$.

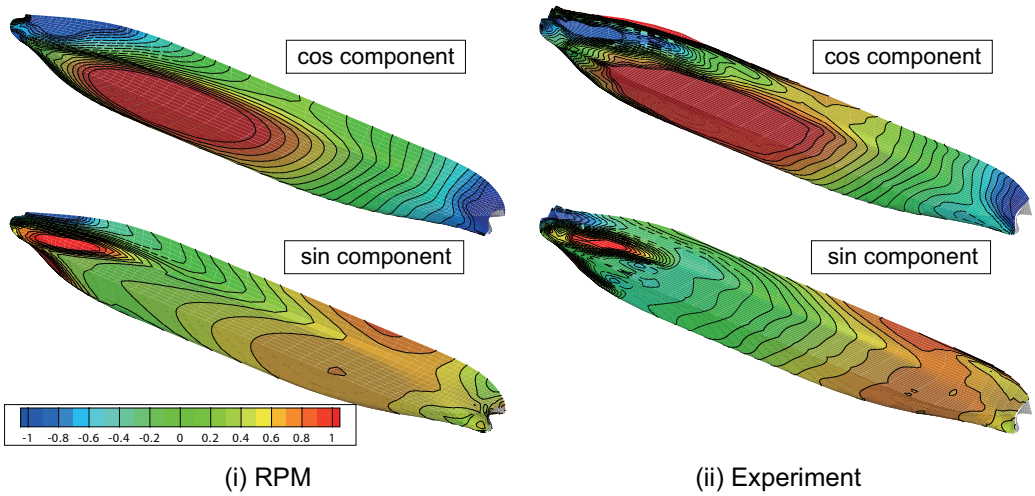

Fig. 7 Unsteady pressure distribution on the ship hull at $F_n = 0.18$, $\beta = 180$ deg and $\lambda/L = 1.25$.

5.4 Added Pressure

Figure 8 (a) shows measured and computed added resistance, and Fig. 8 (b) shows the measured added pressure distributions at three representative wavelengths that are obtained as the difference of steady pressures in calm water and in waves. The added pressure in bow part is larger than that in other parts, which means that the bow part especially near the water surface contributes to the added resistance dominantly.

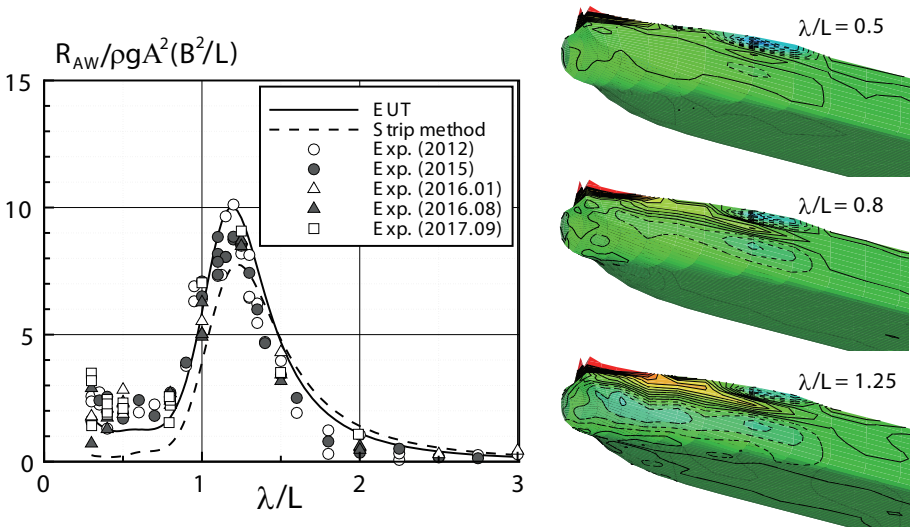

(a) Added resistance (b) Added pressure distribution

Fig. 8 Added resistance and added pressure distributions on RIOS bulk carrier at $F_n = 0.18$ and $\beta = 180$ deg.

6 CONCLUSION

The pressure distributions measured with a large number of FBG pressure sensors were compared with calculation results by the strip method, the enhanced unified theory, and the Rankine panel method in order to demonstrate its usefulness for validating the calculation methods. Through the present study, it was shown that the measurement with FBG pressure sensors is accurate enough and valuable as the validation data for any computation method. The measurement in oblique waves using the present method and a comparison of obtained results with advanced CFD will be future work.

REFERENCES

1) Iwashita, H., Kashiwagi, M., Ito, Y., Seki, Y., Yoshida, J., Wakahara, M.: Calculation of Ship Seakeeping in Low-Speed/Low-Frequency Range by Frequency-Domain Rankine Panel Methods (in Japanese), Journal of The Japan Society of Naval Architects and Ocean Engineers, No.24, pp. 129-146, 2017.

2) Kashiwagi, M.: Prediction of Surge and its Effects on Added Resistance by Means of the Enhanced Unified Theory, Transactions of the West-Japan Society of Naval Architects, No.89, pp. 77-89, 1995.

3) Iwashita, H.: On Numerical Treatments of the Infinite Condition in the Frequency-Domain Rankine Panel Method (in Japanese), Journal of The Japan Society of Naval Architects and Ocean Engineers, No.24, pp. 105-127, 2017.